Journal of Biomedical Optics 8(2), 264–272 (April 2003)

Optoacoustic determination of optical attenuation depth using interferometric detection

Barry P. Payne
Massachusetts Institute of Technology
Department of Mechanical Engineering
Cambridge, Massachusetts 02139
and
Massachusetts General Hospital
Wellman Laboratories of Photomedicine
Boston, Massachusetts 02114

Vasan Venugopalan, MEMBER SPIE
University of California, Irvine
Department of Chemical Engineering and
Materials Science and
Laser Microbeam and Medical Program
Beckman Laser Institute
916 Engineering Tower
Irvine, California 92697-2575
vvenugop@uci.edu

Bora B. Mikić
Massachusetts Institute of Technology
Department of Mechanical Engineering
Cambridge, Massachusetts 02139

Norman S. Nishioka, MEMBER SPIE
Massachusetts General Hospital
Wellman Laboratories of Photomedicine
Boston, Massachusetts 02114

Abstract. We use a modified Mach-Zehnder interferometer to measure surface displacement resulting from the thermoelastic response of a target to the absorption of a short laser pulse with axial and temporal resolutions of 0.1 nm and 3 ns, respectively. These measurements are used in conjunction with a solution to the thermoelastic wave equation and a nonlinear optimization algorithm to extract optical attenuation depth. We demonstrate the ability to determine the effective optical attenuation depth of homogeneous targets with either diffuse or specular reflecting surfaces with a precision of ⩽4% for attenuation depths spanning 0.1 to 2 mm. [DOI: 10.1117/1.1559731]

Keywords: photoacoustic; thermoelastic; optical diagnostics; optical properties.

Paper 01070 received Oct. 18, 2001; revised manuscript received Jun. 20, 2002; accepted for publication Oct. 7, 2002.

1 Introduction

Tissue optical properties play a central role in the application of light for medical diagnostics and therapeutics. For example, application of laser surgery and photodynamic therapy relies on the achievement of specific spatial distributions of laser energy within the tissue, that is in turn governed by tissue optical properties. Measurement of optical properties also yields diagnostic information regarding the metabolic, physiologic, and structural state of tissue. In many applications, an effective optical attenuation depth is used to characterize light dosimetry within tissues. The effective attenuation depth is the reciprocal of the optical absorption coefficient for nonscattering media, and is a function of the absorption coefficient, scattering coefficient, and single scattering anisotropy for turbid media.[1,2]

Several optical methods are available to measure the effective attenuation depth of light within tissue. These methods typically employ optical transmittance and/or reflectance measurements in conjunction with a radiative transport model to estimate optical properties. These techniques can be performed in spatial, temporal, or frequency domains. When using spatially resolved methods, light of constant intensity is launched into tissue and detected at several spatial locations.[3–5] When using time-domain or time-resolved methods, a pulse of light is launched into tissue, and changes in the pulse shape resulting from its propagation are used to extract optical absorption and scattering properties. In this case, a single source-detector pair is sufficient to characterize the optical properties.[6–8] The third approach uses high-frequency intensity-modulated light to create diffuse photon density waves (PDW) that propagate in tissue with a wave vector that is a function of optical properties.[9–14]

Optoacoustic techniques can also be employed to determine optical properties of turbid media.[15–17] Optoacoustic techniques typically measure the thermoelastic stresses generated by the absorption of a short laser pulse. These stresses are a function of the spatial distribution of absorbed energy and are therefore dependent on the optical properties of the sample. Current optoacoustic techniques employ transducers placed in contact with the target to measure these stresses. In many cases, the measurement must be made on the same surface as the laser exposure, because access to both sides of the tissue target is not possible. Thus transducers that are placed on the front surface of the target can be impractical, because they block the incident laser light. A variety of techniques have been used to overcome this difficulty, including the use of piezoelectric transducers with separated light and sound fields, transparent transducers that measure pressure-induced changes in optical reflectance, and annular piezoelectric elements and acoustic conductors where the stresses generated by an obliquely incident laser pulse propagates predominantly normal to the tissue surface.[15,16,18–22] Despite these advances, stress detection using sensors placed in contact with the tissue may be impractical in some medical applications and may not be compatible with minimally invasive procedures.

In this work, a minimally invasive noncontact interferometric technique is used to accurately measure the effective

1083-3668/2003/$15.00

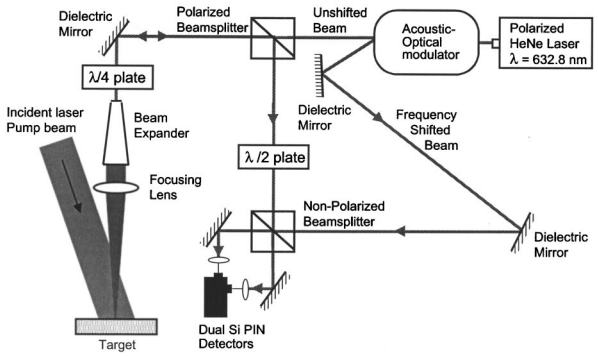

Fig. 1 Interferometer used to measure surface displacement.

optical attenuation depth of a sample. This technique measures the time-resolved surface displacement resulting from absorption of a short laser pulse. The surface motion is caused by thermoelastic stress relaxation, whose time constant is proportional to the optical attenuation depth of the sample. The magnitude of expansion is a function of the incident radiant exposure and thermophysical properties of the sample. This technique is complementary to interferometric photothermal spectroscopy, a method that determines the effective optical attenuation depth through time-resolved measurement of surface displacement resulting from the thermal diffusion that follows the thermoelastic stress relaxation process.[23,24] The use of an interferometric system to calculate optical attenuation depth by measuring surface motion has been described previously[25–28] and used to make preliminary attenuation depth measurements of human meniscal cartilage.[29]

2 Interferometer System

2.1 *Interferometer Design*

The interferometer system is shown in Fig. 1 and represents a refined version of a system described previously.[24] A polarized helium-neon (He-Ne) laser beam (Melles Griot, Irvine, California) with a wavelength of 632.8 nm was used as the interferometric probe beam. An acousto-optic modulator (AOM, IntraAction Corporation, Bellwood, Illinois) deflected the beam and imparted a frequency shift of 110 MHz to the reference beam. The unshifted (sample) beam is passed through a polarized beamsplitter and directed to the target through a quarter waveplate. When necessary, a 10× beam expander (Melles Griot) and 80-mm focal-length gradient-index lens can be used to increase the numerical aperture to yield a spot size of 10 μm. The reflected He-Ne laser beam is passed back through the quarter waveplate, thereby rotating the polarization state of the sample beam by 90 deg, and causing it to be reflected by the polarization-sensitive beamsplitter. The sample beam is passed through a half waveplate to restore the original state of polarization and is recombined with the reference beam by a 50/50 beamsplitter. The recombined beams have a 180 deg phase difference and are focused by 25.4-mm focal length lenses onto two Si PIN photodiodes (Hamamatsu, Bridgewater, New Jersey). The small active area of the PIN diodes (0.126 mm^2) act as pinholes and provide confocal detection of the target surface. The photocurrents generated by the Si PIN photodiodes are subtracted and cancel any inherent laser noise. The subtracted photodiode current is amplified by a commercial 500-MHz broadband low-noise amplifier (Mini-Circuits, Branson, Missouri) and digitized by a 500-MHz bandwidth oscilloscope (Tektronix, Wilsonville, Oregon). When the sample surface is stationary, the photodiodes detect interference fringes that oscillate at the modulation frequency of 110 MHz. When the sample surface moves, the path length difference between the two arms changes and the phase of the modulation frequency is altered. The polarity of the phase shift is dependent on the direction of sample movement. The intensity reaching the photodiodes is a function of time t, path length difference δ, and the sample and reference beam intensities, and is given by:

$$I(\delta,t)=I_1+I_2+2\sqrt{I_1 I_2}\cos(\phi_m), \tag{1}$$

where I_1 and I_2 are the intensities of the sample beam and reference beam. ϕ_m is the phase of the modulated signal:

$$\phi_m=k\delta+\Delta wt, \tag{2}$$

where k is the propagation vector and Δw is the modulation frequency. The surface displacement $S(t)$ is equal to half the path length difference and given by:

$$S(t)=\frac{\delta}{2}=\frac{\phi_m-\Delta wt}{2k}=\frac{\phi_m-\phi_{AOM}}{2k}. \tag{3}$$

The surface displacement is computed by subtracting the phase of the AOM drive signal from the phase of the detected signal. The phase of both signals is obtained using the Hilbert transform.

2.2 *Interferometer Performance*

The interferometer shown here was inspired by an original design presented by Albagli coworkers.[27] In this original design, a moving mirror placed in the reference arm was used to accomplish the frequency shift in the reference beam, a single photomultiplier tube was used for detection, and no polarization-sensitive optics were used. The standard deviation of the baseline traces obtained from this interferometer design was approximately 4 nm.

A few years later, Yablon and coworkers demonstrated a modified interferometer design that reduced the baseline standard deviation by a factor of four. Their instrument employment an AOM instead of a moving mirror to accomplish the frequency shift in the reference arm, polarization-sensitive optics to improve the strength of the optical signal, and an avalanche photodiode for detection.[24] The performance of the present interferometer is best illustrated by comparing a surface displacement trace with one obtained using this earlier interferometer that did not employ dual PIN diode detection.[24] Surface displacement traces of colored glass after Q-switched Nd:YAG laser irradiation at 355 nm are shown in Fig. 2. Both traces were obtained under similar conditions. The axial resolution as defined by the standard deviation (STD) of the displacement signal has been improved by an order of magnitude from 0.93 to 0.09 nm. The maximum displacement in both cases was approximately 30 nm.

In general, there is a tradeoff between the temporal and spatial resolution provided by the interferometric system. Although subnanosecond temporal resolution is possible, we ap-

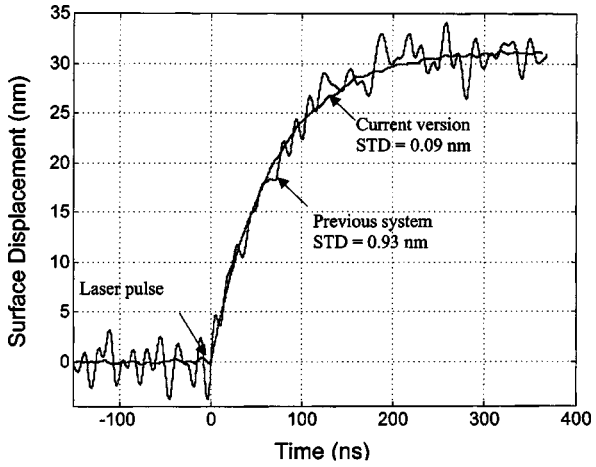

Fig. 2 Comparison of surface expansion traces of colored glass during Q-switched Nd:YAG laser irradiation at λ=355 nm.

plied an 80-MHz bandpass filter centered at 110 MHz to all displacement traces to eliminate high-frequency noise and limit our signal to record velocities that are physically possible. This resulted in displacement traces with a 4-ns temporal resolution and STD that varied between 0.08 nm for targets with specularly reflecting surfaces to 0.16 nm for diffusely reflecting targets.

3 Theoretical Modeling

The one-dimensional time-resolved surface expansion resulting from the absorption of an instantaneous laser pulse is derived in Sec. 8 and given by:

$$S(t)=S_0\left[1-\exp\left(-\frac{c_L}{D}t\right)\right], \tag{4}$$

where

$$S_0=\frac{\beta K\theta_0 D}{\rho c_L^2}=\frac{\beta\theta_0 D}{3}\left(\frac{1+\nu}{1-\nu}\right)=\frac{\beta\phi_0(1-R_s)}{3\rho c_v}\left(\frac{1+\nu}{1-\nu}\right), \tag{5}$$

where β is the coefficient of thermal expansion, K is the bulk modulus, θ_0 is the relative surface temperature, D is the effective optical attenuation depth, ρ is the density, c_L is the longitudinal sound speed, ν is the Poisson's ratio, ϕ_0 is the incident radiant exposure, R_s is the specular reflectance, and c_v is the specific heat capacity at constant volume.

When the pump laser pulse has a finite duration, the impulse solution must be convolved with the temporal profile of the incident radiation. The temporal profile of the laser pulse used in all experiments resembled a Gaussian distribution. The one-dimensional surface displacement caused by the absorption of such a laser pulse is derived in Sec. 9 and given by:

Table 1 Physical properties of Schott neutral density glass samples.

Glass type	Young's modulus (GPa)	Poisson ratio	Density (kg/m^3)	Speed of sound (m/s)
NG1	62	0.229	2490	5370
NG10	62	0.229	2470	5390
NG9	62	0.229	2440	5420
NG3	62	0.229	2440	5420
NG4	62	0.227	2430	5430
NG5	62	0.229	2430	5430

$$S(t)=\frac{\beta\phi_0(1-R_s)}{6\rho c_v}\left(\frac{1+\nu}{1-\nu}\right)\left\{1+\mathrm{erf}(a^{1/2}t)-\exp\left(-\frac{d^2}{4a}\right)\exp(-dt)\left[1+\mathrm{erf}\left(\frac{2at-d}{4a}\right)\right]\right\}, \tag{6}$$

where

$$a\equiv\frac{2.8}{\mathrm{FWHM}^2}, \tag{7}$$

where FWHM is the full width at half maximum of the laser temporal profile and $d\equiv(c_L/D)$.

4 Materials and Methods

4.1 *Measurement of Colored Glass*

To validate this technique, a set of well-characterized absorbing neutral density glass samples (Schott Glass Technologies Incorporated, Duryea, Pennsylvania) were measured. Optical and thermal properties were obtained from the manufacturer and are listed in Table 1. A Q-switched Nd:YAG laser was frequency doubled to operate at 532 nm and used as the pump laser. The laser pulse possessed a Gaussian temporal profile with a FWHM duration of 7 ns. The spatial profile, analyzed using a CCD camera (Cohu 4800, Cohu Incorporated), resembled a flat top with a FWHM diameter of 6 mm. The angle of incidence of the pump laser at the sample was 15 deg. The refractive index of glass is 1.5 and results in the propagation of the pump laser pulse within the glass at an angle of 10 deg. The measured attenuation depth was corrected by dividing the measured value by cos(10 deg). A diagram of the experimental setup is shown in Figure 3. The interferometer probe beam was centered within the incident pump beam on the target surface. The incident radiant exposures used were 10 to 550 mJ/cm^2.

4.2 *Measurement of Gelatin Phantoms*

To demonstrate the use of this technique on diffusely reflecting targets, the surface displacement of gelatin phantoms doped with potassium chromate (K_2CrO_4, Aldrich Chemical Company, Milwaukee, Wisconsin) was measured. Potassium chromate was used to increase optical absorption of the phan-

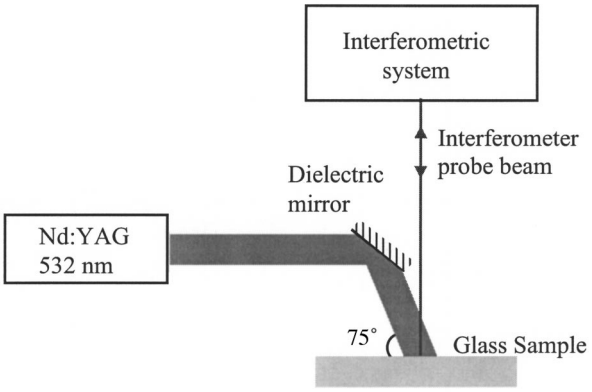

Fig. 3 Schematic of experimental setup to determine optical attenuation depth using interferometric detection.

tom. This was done to provide a geometry wherein the effective optical attenuation depth of the pump laser radiation was much smaller than the diameter of the pump laser beam, and to ensure validity of the one-dimensional modeling treatment given in §3. Potassium chromate was selected, as its absorption properties are known to be photochemically stable.[16,21]

The experimental setup was similar to the setup used in the colored glass experiments described in § 4.1. The Q-switched Nd:YAG pump laser was operated at its third harmonic with a wavelength of 354.7 nm. The spatial profile resembled a top hat with FWHM diameter of 6 mm. The temporal profile was Gaussian in shape with FWHM duration of 8 ns. When measuring surface displacements on diffusely reflecting samples, a smaller interferometer spot size is required to ensure that sufficient coherent light is reflected. The incident radiant exposure was 70 mJ/cm^2.

Three different solutions of potassium chromate were prepared with molar concentrations of 0.0188, 0.0169, and 0.0154 M, yielding estimated attenuation depths of 95, 106, and 117 μm, respectively. All solutions were prepared with distilled water and filtered. Tissue phantoms were prepared by mixing 10% gelatin (G-1890 Type A gelatin, Sigma, Saint Louis, Missouri) by weight with a 0.0169-M potassium chromate solution.

5 Results

5.1 *Measurement of Colored Glass*

A sample displacement trace for a glass sample with the best-fit solution is shown in Fig. 4. A single pulse from the Nd:YAG pump laser was absorbed by the glass sample beginning at 0 ns, generating thermoelastic stresses within the glass sample. These stresses propagated through the glass, reflected off the free surface, and produced a surface displacement that is a function of effective optical attenuation depth D and longitudinal sound speed c_L of the target. The glass sample was stationary prior to the delivery of the laser pulse. At times greater than 300 ns, shear waves influenced the surface profile, making a one-dimensional treatment of the thermoelastic stress dynamics invalid. The maximum surface displacement was 45 nm. The best-fit trace was obtained by performing a Gauss-Newton least-squared optimization of Eq. (6), with the maximum displacement and the effective attenuation depth D

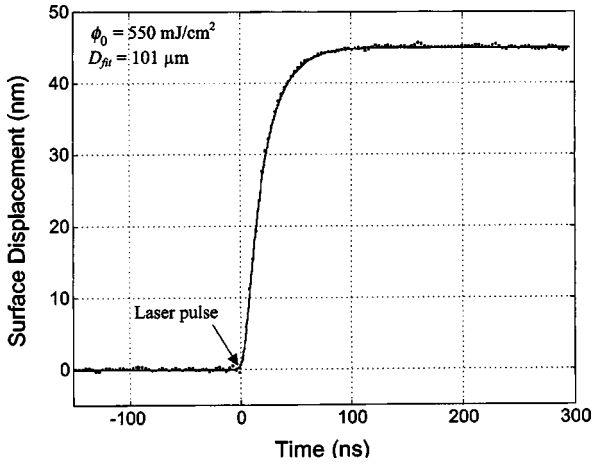

Fig. 4 Sample displacement trace and best-fit solution for Schott glass type NG1. The symbols represent the interferometer data taken at a sampling rate of 2 GS/s, of which only 1 of every 6 points is shown for clarity.

as floating parameters. The best-fit trace corresponds to an optical attenuation depth of 101 μm and is in good agreement with the known properties of the target.

The measurements were repeated for incident radiant exposures ranging from 12 to 440 mJ/cm^2. The displacement traces and best-fit curves are shown in Fig. 5. Figure 6 shows surface displacement traces with best-fit solutions for all Schott glass samples tested. The incident radiant exposure was 550 mJ/cm^2. For ease of comparison, the maximum displacements have been normalized. Table 2 summarizes the measured optical penetration depths (mean$\pm$one standard deviation) for all glass samples, compared to values computed from transmission curves given by the manufacturer. To evaluate the reproducibility of the results, the attenuation depth of the NG 9 glass was determined from 350 separate surface displacement traces. The traces were obtained over a

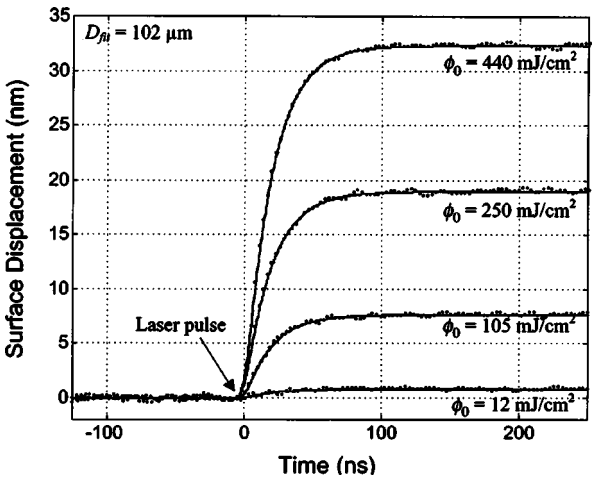

Fig. 5 Sample displacement traces and best-fit solutions for Schott glass type NG1. The incident radiant exposure ranged from 12 to 440 mJ/cm^2. The symbols represent the interferometer data taken at a sampling rate of 2 GS/s, of which only 1 of every 6 points is shown for clarity.

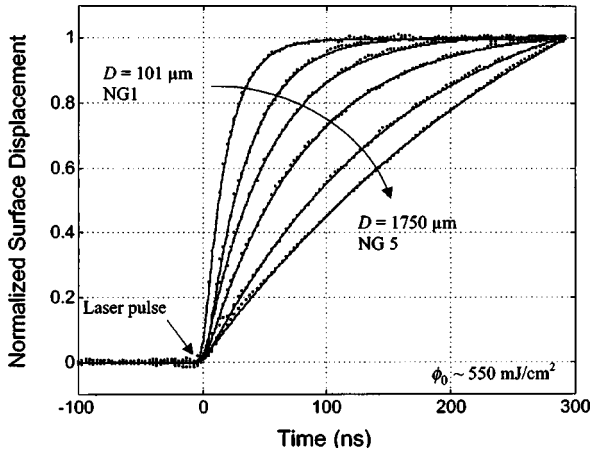

Fig. 6 Sample displacement traces with best-fit solutions for all Schott glass samples used. The symbols represent the interferometer data taken at a sampling rate of 2 GS/s, of which only 1 of every 6 points is shown for clarity.

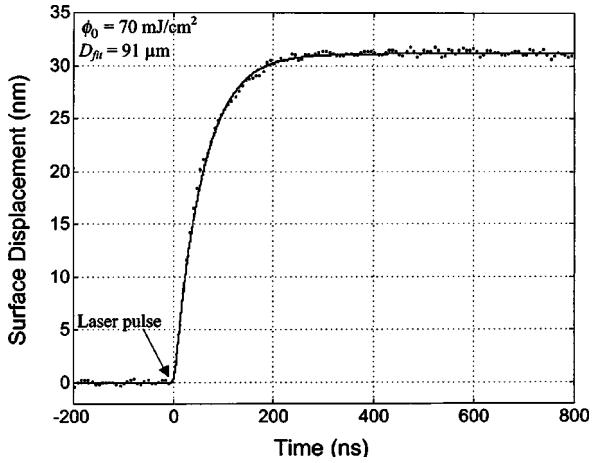

Fig. 7 Sample displacement trace and best-fit solution for a 0.0169-M potassium chromate solution. The symbols represent the interferometer data taken at a sampling rate of 2 GS/s, of which only 1 of every 14 points is shown for clarity.

period of two months under different operating and alignment conditions. The resulting values for optical attenuation depth varied by no more than 0.6%.

5.2 *Measurement of Gelatin Phantoms*

A sample displacement trace and best-fit solution for a 0.0169-M potassium chromate solution is shown in Fig. 7. The best-fit solution matched the measured displacement trace and had an attenuation depth of 91 μm compared with the estimated value of 106 μm. Table 3 summarizes results for three potassium chromate solutions. These results show excellent agreement between IPMS and the estimated values of effective attenuation depth. The molar attenuation coefficient determined from the extracted effective attenuation depth is 2798 $M^{-1}\,cm^{-1}$ and is consistent with both values estimated from the literature (2410 $M^{-1}\,cm^{-1}$), and obtained via standard transmission experiments (2800 $M^{-1}\,cm^{-1}$).

A sample displacement trace and best-fit solution for a gelatin phantom doped with a 0.0169-M potassium chromate solution is shown in Fig. 8. The best-fit solution matched the measured displacement trace with an effective attenuation depth of 136 μm. This attenuation depth was higher than the attenuation depth of the 0.0169-M potassium chromate solution alone (91 μm). The effective attenuation depth of gelatin-doped tissue phantoms appeared to decrease with repeated laser pulses. Although this decrease was small, it was clearly detectable. Figure 9 compares the calculated effective attenuation depth for a 0.0169-M potassium chromate solution with a gelatin phantom prepared with the same solution.

Table 2 Measured optical attenuation depths for Schott neutral density glass samples compared with values obtained from Schott Glass Technologies.

Glass type (λ=532 nm)	Measured attenuation depth (60 points)	Schott given attenuation depth
NG1	101± 0.8μm	106± 50μm
NG10	187± 1.5μm	188± 11μm
NG9	305± 2.2μm	306± 50μm
NG3	435± 3.5μm	434± 40μm
NG4	858±10 μm	856± 70μm
NG5	1780±80 μm	1790±170μm

6 Discussion

6.1 *Instrumentation*

We have designed and built a high-resolution interferometric system capable of measuring surface deformation with angstrom displacement and subnanosecond temporal resolution. The displacement resolution of this system was 10 to 50 times better than those obtained by previous investigators.[24–29] The current system could be improved further by increasing the power of the He-Ne probe laser. This would provide shot noise limited detection for targets that provide low-reflectance or possess diffusely reflecting surfaces. For highly reflecting targets, noise calculations indicated that the system was already limited by shot noise. Note that the system could be configured using fiber optic components. This would simplify alignment, increase modulation depth, and enable the system to be used in clinical applications, including minimally invasive catheter-based procedures.

Table 3 Measured optical attenuation depth for three potassium chromate solutions compared with estimated values.

Molar concentration (λ=354.7 nm)	Measured attenuation depth (30 points)	Estimated attenuation depth
0.0188 M	81±2.0μm	95±~50μm
0.0169 M	91±2.2μm	106±~50μm
0.0154 M	100±2.7μm	117±~50μm

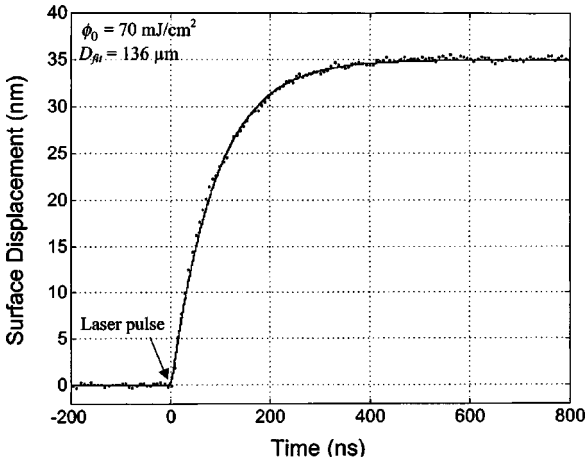

Fig. 8 Sample displacement trace and best-fit solution for a gelatin tissue phantom doped with a 0.0169-M potassium chromate solution. The symbols represent the interferometer data taken at a sampling rate of 2 GS/s, of which only 1 of every 14 points is shown for clarity.

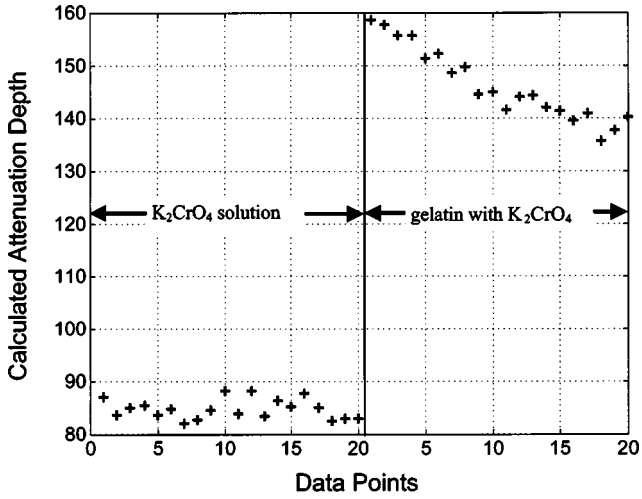

Fig. 9 Calculated attenuation depth for a 0.0169-M potassium chromate solution and calculated attenuation depth for a gelatin tissue phantom prepared with the same solution.

6.2 *Interferometric Determination of Optical Properties*

The accuracy of the proposed interferometric technique was assessed via measurement of the effective attenuation depth of well-characterized absorbing glass samples. The variation in the measured values was generally more than an order of magnitude lower than the range given by the glass manufacturer. In addition, the technique provided consistent results when performed under different alignment and laser operating conditions. The consistently accurate results are primarily due to the high axial and temporal resolution of the interferometer system. The effective attenuation depth is determined by fitting the time-resolved surface displacement measurement to that predicted by a one-dimensional treatment of the thermoelastic wave equation. For purely absorbing samples, this simplified treatment is sufficient so long as the pump laser beam diameter is much larger than the optical penetration depth. This is an attractive feature that eliminates the need for a full three-dimensional treatment of thermoelastic wave propagation to extract the attenuation depth of weakly absorbing samples.

Determination of the effective attenuation depth in optically turbid samples can also be achieved using this approach. In this case, one must employ a pump laser beam whose diameter is much larger than the optical transport mean free path of the target. If this additional condition is not satisfied, the light distribution within the sample will have a three-dimensional character and will result in an underestimation of the effective attenuation depth. In the future, it may be possible to extract both absorption μ_a and reduced scattering μ_s' coefficients or accommodate spatially heterogeneous media by incorporating a different formulation for the spatial distribution of the absorbed radiation or by explicit consideration of the inverse problem in the form of an integral equation.[30] In situations where the optical properties of the sample are known, the maximum surface displacement could be used to extract other properties of the target, such as the thermal expansion coefficient, Poisson ratio, density, and/or specific heat capacity.

This technique was also used to investigate laser-induced surface deformation of gelatin tissue phantoms. The best displacement resolution achieved on these diffusely reflecting surfaces was 0.16 nm. The slight deterioration in displacement resolution was a consequence of the reduced amount of light reflected from the gelatin surfaces in comparison to the glass samples. The effective optical attenuation depth was found to decrease with the number of additional laser pulses. The attenuation depth and its rate of decrease appeared to be a function of gelatin type, potassium chromate concentration, and incident radiant exposure. Explanations for these effects may include photochemical processes, dehydration, or laser-induced changes in the optical properties of the phantom. Although these effects resulted in a small change in the attenuation depth of the gelatin phantom, they were clearly detectable. These effects may be important when preparing tissue phantoms for the testing and validation of new techniques or applications.

The use of radiant exposures as large as 550 mJ/cm^2 to obtain the measured displacement traces may attract attention, as these exposures are 5.5 times greater than those allowed by the ANSI standard.[31] However, these measurements were made in the colored glass samples, a material that expands approximately six times less than water or tissue for an identical radiant exposure. In fact, for the gelatin-based phantoms, the largest radiant exposure used was 70 mJ/cm^2. These exposures resulted in maximum displacements of approximately 35 nm and were more than ample to obtain accurate determinations of the effective optical attenuation depth.

The challenge of diagnostic spectroscopy is to measure changes in optical properties, such as effective attenuation depth, and correlate these changes with specific changes in tissue state. Often, changes in the optical properties are subtle, and must therefore be measured with a high-resolution technique. The interferometric technique shown here provides high resolution and is capable of differentiating small changes in attenuation depth ($\sim$5 μm). In addition, the system could be fabricated using fiber optic compatible instrumentation and

used as a clinically valuable minimally invasive diagnostic tool.

7 Conclusions

We have demonstrated the use of an interferometric system to determine the effective optical attenuation depth of homogenous samples by measuring the optoacoustic response to the absorption of a short laser pulse. The system measures the time-resolved surface displacement that is a function of the thermal, mechanical, and optical properties of the target. We have successfully used this technique to measure effective optical attenuation depths ranging from 0.1 to 2 mm in both diffusely and specularly reflecting targets with high precision. We expect that the application of this technique will be extended to measure optical absorption and scattering coefficients in homogeneous and heterogeneous turbid media.

8 Appendix A

We derive the relationship between surface displacement and optical attenuation depth of a sample after absorption of a laser impulse. The following derivation is based on the linear theory of elasticity.[32,33]

The stress tensor, the equation of motion, and the constitutive relation for the material govern the stress and strain relationship of any material. The effects of thermal diffusion were neglected because the time scale for stress relaxation is much more rapid compared to the time scale for thermal diffusion. The strain tensor (ε_{ij}) is given by Eq. (8) and is the small strain approximation of the Lagrangian strain tensor (η_{ij}). The subscripts represent standard indicial notation.

$$\eta_{ij} \approx \varepsilon_{ij} = \tfrac{1}{2}(u_{i,j} + u_{j,i}), \tag{8}$$

where u_i is the displacement vector. The equation of motion is derived from the conservation of momentum and given by:

$$\sigma_{ij,j} + b_i = \rho \dot{V}_i, \tag{9}$$

where σ_{ij} is the stress tensor, b_i is the body force vector, ρ is the density, and $\dot{V}_i$ is the acceleration vector. The constitutive relation for a linear isotropic material is given by:

$$\varepsilon_{ij} = \frac{1+\nu}{E}\sigma_{ij} - \frac{\nu}{E}\sigma_{kk}\delta_{ij} + \beta\theta\delta_{ij}, \tag{10}$$

where ν is Poisson's ratio, E is the elastic modulus, β is the coefficient of thermal expansion, θ is the relative temperature, and δ_{ij} is the Kronecker delta. Assuming the laser energy is absorbed exponentially, the temperature distribution will be:

$$\theta = \theta_0 \exp(-z/D), \tag{11}$$

where θ_0 is the relative surface temperature, and D is the effective optical attenuation depth, which for purely absorbing samples, is equal to the inverse of the absorption coefficient. Substituting Eqs. (11) and (10) into Eq. (9), we obtain the partial differential equation for displacement as a function of depth z and time t.

$$\frac{\partial^2 u}{\partial z^2} - \frac{1}{c_L^2}\frac{\partial^2 u}{\partial t^2} = -\frac{\beta K \theta_0}{\rho c_L^2 D}\exp(-z/D), \tag{12}$$

where c_L is the longitudinal speed of sound and K is the bulk modulus given by:

$$c_L^2 \equiv \frac{E(1-\nu)}{\rho(1+\nu)(1-2\nu)} \tag{13}$$

and

$$K \equiv \frac{E}{3(1-2\nu)}. \tag{14}$$

The initial conditions and boundary conditions are:

$$\begin{aligned} u &= 0 \quad \text{at } t = 0, \\ \frac{\partial u}{\partial t} &= 0 \quad \text{at } t = 0, \\ \sigma &= 0 \quad \text{at } z = 0, \\ u &= 0 \quad \text{as } z \to \infty. \end{aligned} \tag{15}$$

The solution can be obtained using the Laplace integral transform method:

$$L\{f(t)\} = \overline{f}(p) = \int_0^\infty \exp(-pt) f(t)\, dt. \tag{16}$$

Transforming Eq. (12) into the Laplace domain yields

$$q^2 \overline{u} = \frac{\partial^2 \overline{u}}{\partial z^2} + \frac{Q}{p}\exp(-z/D), \tag{17}$$

where

$$Q = \frac{\beta K \theta_0}{D\rho c_L^2} \quad \text{and} \quad q = \frac{p}{c_L}. \tag{18}$$

The general solution is given by:

$$\begin{aligned} \overline{u} = {} & C_1 \exp(-qz) + C_2 \exp(-qz) \\ & + \frac{Q}{p}\left[\frac{D^2}{q^2 D^2 - 1}\right]\exp(-z/D). \end{aligned} \tag{19}$$

Solving for the constants of integration C_1 and C_2 by applying the boundary conditions of Eq. (15) yields the final solution in the Laplace domain:

$$\overline{u} = \frac{QDc_L}{p^2 - \gamma^2}\exp(-qz) + \frac{QD^2\gamma^2}{p(p^2-\gamma^2)}\exp(-z/D), \tag{20}$$

where

$$\gamma = \frac{c_L}{D}. \tag{21}$$

The final solution is transformed back into the time domain using the following relationships:

$$L\begin{Bmatrix} 0, & t < \alpha \\ f(t-\alpha), & t \leqslant \alpha \end{Bmatrix} = \exp(-\alpha p)\overline{f}(p),$$

$$L\{1\}=\frac{1}{p} \quad \text{and} \quad L\{\exp(-\alpha t)\}=\frac{1}{p+\alpha}. \tag{22}$$

The one-dimensional surface displacement is thus given by:

$$u(z,t)=\frac{\beta K\theta_0 D}{2\rho c_L^2}\left\{\exp\left[-\frac{c_L}{D}\left(t-\frac{z}{c_L}\right)\right] + \exp\left[-\frac{c_L}{D}\left(t+\frac{z}{c_L}\right)\right]-2\exp(-z/D)\right\}$$

$$\text{for} \quad t\geqslant\frac{z}{c_L} \tag{23}$$

and

$$u(z,t)=\frac{\beta K\theta_0 D}{2\rho c_L^2}\left\{\exp\left[\frac{c_L}{D}\left(t-\frac{z}{c_L}\right)\right]+\exp\left[-\frac{c_L}{D}\left(t+\frac{z}{c_L}\right)\right] -2\exp(-z/D)\right\} \quad \text{for} \quad t<\frac{z}{c_L}. \tag{24}$$

At the surface $(z=0)$, the solution simplifies to:

$$S(t)=-u(z=0,t)=S_0\left[1-\exp\left(-\frac{c_L}{D}t\right)\right], \tag{25}$$

where

$$S_0=\frac{\beta K\theta_0 D}{\rho c_L^2}=\frac{\beta\theta_0 D}{3}\left(\frac{1+\nu}{1-\nu}\right)=\frac{\beta\phi_0(1-R_s)}{3\rho c_v}\left(\frac{1+\nu}{1-\nu}\right), \tag{26}$$

where ϕ_0 is the incident radiant exposure, R_s is the specular reflectance, and c_v is the specific heat at constant volume.

9 Appendix B

Here we derive the relationship between surface displacement and attenuation depth of a sample after absorption of a laser pulse of finite duration. To do so the impulse solution must be convolved with the temporal profile of the laser pulse:

$$S(t)=S_0\int_0^\infty[1-\exp(-dx)]g(x-t)dx, \tag{27}$$

where $d\equiv c_L/D$ and $g(x)$ is the temporal profile of the laser pulse. The temporal profile of the laser pulse used in this study resembled a Gaussian function and is given by:

$$g(x)=\sqrt{\frac{a}{\pi}}\exp(-ax^2), \tag{28}$$

where

$$a\equiv\frac{2.8}{\text{FWHM}^2}. \tag{29}$$

FWHM is the full width half max of the laser temporal profile. Solving Eq. (27) yields the final one-dimensional surface displacement caused by the finite laser pulse:

$$S(t)=\frac{\beta\phi_0(1-R_s)}{6\rho c_v}\left(\frac{1+\nu}{1-\nu}\right)\left\{1+\text{erf}(a^{1/2}t) - \exp\left(-\frac{d^2}{4a}\right)\exp(-dt)\left[1+\text{erf}\left(\frac{2at-d}{4a}\right)\right]\right\}. \tag{30}$$

Acknowledgments

The authors wish to thank Hans Ludemann, Brett Bouma, Gary Tearney, and Andrew Yablon for advice and technical assistance. This research was made possible by the DOD Medical Free Electron Laser Program N00014-94-1-0927, the Office of Naval Research DAAH04-95-1-0216, U.S. Army grant USAMRAAD DAMD 1794C4009, and NIH Laser Microbeam and Medical Program NIH-NCRR-01192.

References

1. B. C. Wilson and S. L. Jacques, ''Optical reflectance and transmittance of tissues—Principles and applications,'' *IEEE J. Quantum Electron.* **26**, 2186–2199 (1990).
2. W. F. Cheong, S. A. Prahl, and A. J. Welch, ''A review of the optical-properties of biological tissues,'' *IEEE J. Quantum Electron.* **26**, 2166–2185 (1990).
3. E. L. Hull, M. G. Nichols, and T. H. Foster, ''Quantitative broadband near-infrared spectroscopy of tissue-simulating phantoms containing erythrocytes,'' *Phys. Med. Biol.* **43**, 3381–3404 (1998).
4. T. J. Farrell, M. S. Patterson, and B. Wilson, ''A diffusion theory model of spatially resolved, steady-state diffuse reflectance for the noninvasive determination of tissue optical properties in vivo,'' *Med. Phys.* **19**, 879–888 (1992).
5. J. S. Dam, P. E. Andersen, T. Dalgaard, and P. E. Fabricius, ''Determination of tissue optical properties from diffuse reflectance profiles by multivariate calibration,'' *Appl. Opt.* **37**, 772–778 (1998).
6. S. L. Jacques, ''Time-resolved reflectance spectroscopy in turbid tissues,'' *IEEE Trans. Biomed. Eng.* **36**, 1155–1161 (1989).
7. M. S. Patterson, B. Chance, and B. C. Wilson, ''Time resolved reflectance and transmittance for the non-invasive measurement of tissue optical properties,'' *Appl. Opt.* **28**, 2331–2336 (1989).
8. S. J. Matcher, M. Cope, and D. T. Delpy, ''*In vivo* measurements of the wavelength dependence of tissue-scattering coefficients between 760 and 900 nm measured with time-resolved spectroscopy,'' *Appl. Opt.* **36**, 386–396 (1997).
9. M. S. Patterson, J. D. Moulton, B. C. Wilson, K. W. Berndt, and J. R. Lakowicz, ''Frequency-domain reflectance for the determination of the scattering and absorption properties of tissue,'' *Appl. Opt.* **30**, 4474–4476 (1991).
10. B. J. Tromberg, L. O. Svaasand, T. T. Tsay, and R. C. Haskell, ''Properties of photon density waves in multiple-scattering media,'' *Appl. Opt.* **32**, 607–616 (1993).
11. E. M. Sevick-Muraca, J. S. Reynolds, T. L. Troy, G. Lopez, and D. Y. Paithankar, ''Fluorescence lifetime spectroscopic imaging with measurements of photon migration,'' *Ann. NY Acad. Sci.* **838**, 46–57 (1998).
12. B. Chance, M. Cope, E. Gratton, N. Ramanujam, and B. Tromberg, ''Phase measurement of light absorption and scatter in human tissue,'' *Rev. Sci. Instrum.* **69**, 3457–3481 (1998).
13. M. Gerken and G. W. Faris, ''High-precision frequency-domain measurements of the optical properties of turbid media,'' *Opt. Lett.* **24**, 930–932 (1999).
14. T. H. Pham, O. Coquoz, J. B. Fishkin, E. Anderson, and B. J. Tromberg, ''Broad bandwidth frequency domain instrument for quantitative tissue optical spectroscopy,'' *Rev. Sci. Instrum.* **71**, 2500–2513 (2000).
15. K. P. Köstli, M. Frenz, H. P. Weber, G. Paltauf, and H. Schmidt-Kloiber, ''Optoacoustic infrared spectroscopy of soft tissue,'' *J. Appl. Phys.* **88**, 1632–1637 (2000).
16. A. A. Karabutov, E. V. Savateeva, N. B. Podymova, and A. A. Oraevsky, ''Backward mode detection of laser-induced wide-band ultrasonic transients with optoacoustic transducer,'' *J. Appl. Phys.* **87**, 2003–2014 (2000).

17. A. A. Oraevsky, S. L. Jacques, and F. K. Tittel, ''Measurement of tissue optical properties by time-resolved detection of laser-induced transient stress,'' *Appl. Opt.* **36**, 402–415 (1997).
18. C. Kopp and R. Niessner, ''Optoacoustic sensor head for depth profiling,'' *Appl. Phys. B: Lasers Opt.* **68**, 719–725 (1999).
19. G. Paltauf and H. Schmidt-Kloiber, ''Measurement of laser-induced acoustic waves with a calibrated optical transducer,'' *J. Appl. Phys.* **82**, 1525–1531 (1997).
20. P. C. Beard and T. N. Mills, ''Characterization of post mortem arterial tissue using time-resolved photoacoustic spectroscopy at 436, 461 and 532 nm,'' *Phys. Med. Biol.* **42**, 177–198 (1997).
21. Q. X. Chen, R. J. Dewhurst, P. A. Payne, and B. Wood, ''A new laser-ultrasound transducer for medical applications,'' *Ultrasonics* **32**, 309–313 (1994).
22. P. C. Beard and T. N. Mills, ''Extrinsic optical-fiber ultrasound sensor using a thin polymer film as a low-finesse Fabry-Perot interferometer,'' *Appl. Opt.* **35**, 663–675 (1996).
23. A. D. Yablon, ''Photothermal effects of pulsed laser irradiation of biological tissue,'' PhD Dissertation, Massachusetts Institute of Technology, Cambridge, p. 122 (1997).
24. A. D. Yablon, N. S. Nishioka, B. B. Mikić, and V. Venugopalan, ''Measurement of tissue absorption coefficients by use of interferometric photothermal spectroscopy,'' *Appl. Opt.* **38**, 1259–1272 (1999).
25. D. Albagli, ''Fundamental mechanisms of pulsed laser ablation of biological tissue,'' PhD Dissertation, Massachusetts Institute of Technology, Cambridge, p. 314 (1994).
26. I. Itzkan, D. Albagli, M. L. Dark, L. T. Perelman, C. von Rosenberg, and M. S. Feld, ''The thermoelastic basis of short pulsed laser ablation of biological tissue,'' *Proc. Natl. Acad. Sci. U.S.A.* **92**, 1960–1964 (1995).
27. D. Albagli, M. L. Dark, L. T. Perelman, C. von Rosenberg, I. Itzkan, and M. S. Feld, ''Photomechanical basis of laser ablation of biological tissue,'' *Opt. Lett.* **19**, 1684–1686 (1994).
28. D. Albagli, B. J. Banish, M. L. Dark, G. S. Janes, C. von Rosenberg, L. T. Perelman, I. Itzkan, and M. S. Feld, ''Interferometric surface monitoring of biological tissue to study inertially confined ablation,'' *Lasers Surg. Med.* **14**, 374–385 (1994).
29. M. L. Dark, L. T. Perelman, I. Itzkan, J. L. Schaffer, and M. S. Feld, ''Physical properties of hydrated tissue determined by surface interferometry of laser-induced thermoelastic deformation,'' *Phys. Med. Biol.* **45**, 529–539 (2000).
30. T. E. Milner, D. M. Goodman, B. S. Tanenbaum, and J. S. Nelson, ''Depth profiling of laser-heated chromophores in biological tissues by pulsed photothermal radiometry,'' *J. Opt. Soc. Am. A* **12**, 1479–1488 (1995).
31. D. Sliney and M. Wolbarsht, *Safety with Lasers and Other Optical Sources*, New Plenum Press, New York (1980).
32. L. D. Landau and E. M. Lifshitz, *Theory of Elasticity*, Pergamon Press, Oxford (1986).
33. J. N. Timoshenko and J. N. Goodier, *Theory of Elasticity*, McGraw-Hill, New York (1987).